Electric Power Systems Research 177 (2019) 106014

Contents lists available at ScienceDirect

Electric Power Systems Research

journal homepage: www.elsevier.com/locate/epsr

Improved instantaneous power theory based current harmonic extraction for unbalanced electrical grid conditions

Mehmet Büyük[a], Mustafa İnci[b,*], Adnan Tan[a], Mehmet Tümay[a]

[a] Department of Electrical and Electronics Engineering, Çukurova University, Balcalı, Adana, Turkey
[b] Department of Mechatronics Engineering, İskenderun Technical University, İskenderun, Turkey

ARTICLE INFO

Keywords:
Electrical energy quality
Shunt active power filter
Virtual input signal
Instantaneous power theory
Current harmonics
Reactive power compensation

ABSTRACT

This paper presents a novel harmonic extraction method named as "virtual input signal based instantaneous power theory (VIS-IPT)". In this study, VIS-IPT is tested in a shunt active power filter (SAPF) for improving the performance under unbalanced electrical energy quality issues. In the operational process, VIS-IPT is used to generate the compensation signals consisting of harmonic/reactive currents. In the proposed method, reference signal generation is extracted for each phase, separately. In VIS-IPT, the compensation signals are obtained from the calculated powers through multiple-phase inverse Clark transformation. In this way, it eliminates the drawback of conventional IPT which calculates the undesired average reference under unbalanced situations. Moreover, the additional use of PLL for synchronization is eliminated in the proposed method. In this context, a three-phase SAPF system with nonlinear load groups is constructed and analysed in Matlab/Simulink environment in order to prove the efficacy of the proposed method. In addition, the proposed VIS-IPT method is compared with the conventional IPT method through a variety of case studies. The proposed method is examined under different case studies including balanced/unbalanced/distorted voltage and balanced/unbalanced load conditions. The case studies show that the proposed method has excellent compensation capability performance in comparison with the conventional method.

1. Introduction

In recent years, many industrial plants have the rising usage of power electronic based devices such as controlled/uncontrolled rectifiers, variable frequency driver and arc furnaces. These devices draw nonlinear currents from the electric grids, which has brought about pollution of the electric grid network. In the electric grids, the harmonic components circulate throughout electric power systems, which results in a reduction of electric energy efficiency due to power losses, malfunction of control systems, disturbance on the communication network, etc. [1–3]. In order to solve these power quality problems at grid-side, there are several power electronic based custom power devices. Shunt active power filters (SAPF) are the most common devices utilized to attenuate the current based power quality problems. SAPFs are connected in parallel with nonlinear loads and widely used equipment in industrial plants to compensate the harmonic components generated by the nonlinear loads, and thus to satisfy the limits determined in IEEE-519 and IEC EN 61000-3 standards [4,5]. In addition to harmonic compensation, SAPF is also utilized for reactive power compensation to ensure only active energy consumed from the electric grid [6,7].

The control strategy of SAPF is one of the most crucial parts in compensation performance of the harmonics and reactive power. The reference generation of compensation signal plays an important role in the control strategy of SAPF [8–11]. Many reference generation methods in time-domain and frequency-domain have been proposed in the literature such as instantaneous power theory (IPT) [12], synchronous reference frame [13], FFT [14], SDFT [15] and Wavelet transform [16]. Among these methods, IPT is acknowledged as one of the most popular methods. IPT has been implemented to control harmonic and reactive issues in the electric grid network. There are several IPT frameworks in the literature studied by researchers. The basic structure of IPT is discussed by Akagi in Ref. [17]. In this form, the power values in the system are defined as instantaneous zero, real and imaginary power vectors. In Ref. [18], the power vectors of IPT are modified as in-

* Corresponding author.
E-mail addresses: mbuyuk@cu.edu.tr (M. Büyük), mustafa.inci@iste.edu.tr (M. İnci), atan@cu.edu.tr (A. Tan), mtumay@cu.edu.tr (M. Tümay).

https://doi.org/10.1016/j.epsr.2019.106014
Received 31 May 2019; Received in revised form 15 August 2019; Accepted 18 August 2019
Available online 24 August 2019
0378-7796/

stantaneous power and reactive power vectors. Zero and real power vectors are added and considered as instantaneous power. The instantaneous reactive power is divided into imaginary zero, alpha and beta powers. These powers are dependent to each other by a formulation. D–q transformation is considered as modified form of IPT. In d–q transformation, instantaneous active and reactive currents are obtained synchronously with the fundamental frequency [19,20]. A phase locked loop (PLL) is required to perform the synchronization in d–q transformation. In Ref. [21], Verdelho and Soares obtain the synchronization components, cos and sin functions, in αβ frame in order to avoid using PLL. However, third harmonics are generated under unbalanced grid conditions by this way. A different coordinate transformation of IPT was proposed in [7,22]. The current and voltage components are transformed into p–q–r coordinates from αβ coordinates. Several transformations are needed in p–q–r formulation. Recently, enhanced IPT methods have been proposed in [23] and [24]. In Ref. [23], the current and voltage vectors are transformed into another cartesian coordinate system, called *mno* transformation. Then, the powers are calculated in *mno* plane. In Ref. [24], decomposition of current components is performed through positive, negative and zero sequence components. Both methods in [23] and [24] are effective under unbalance conditions. Nevertheless, these methods require many calculations.

In this study, a novel framework of IPT is proposed for distinct electrical grid conditions. The proposed method is based on the generation of virtual signals, namely virtual input signal based instantaneous power theory (VIS-IPT). In the performance stage, a three-phase SAPF system is constructed and analyzed in a simulation environment in order to verify the effectiveness of the proposed method. Also, the proposed method is examined for six different case studies, and compared with the conventional IPT method. The proposed method is tested under balanced/unbalanced/distorted voltage and balanced/unbalanced load conditions. In addition, the proposed method is compared in terms of THD, TDD and PF. The contributions of the paper can be summarized as follows:

- A novel IPT method, called VIS-IPT, has been proposed and presented in detail.
- The mathematical formulations and vector representation of VIS-IPT have been introduced.
- A novel aspect for the generation of cos and sin functions has been presented by using VIS-IPT method. Thus, the use of PLL is eliminated.
- The proposed method has been constructed in SAPF system for harmonic current and reactive power compensation.
- An algorithm has been provided to implement the proposed method.

The rest of the study is organized as follows: the proposed VIS-IPT is introduced in Section 2, consisting of the virtual signal generation and the reference signal generation with the proposed method. Section 3 presents the incorporation of the proposed VIS-IPT method into SAPF for compensation harmonic currents and reactive power. Section IV presents the results of the proposed method with a designed SAPF system in Matlab/Simulink platform by considering six different cases. Besides, the section illustrates various waveforms and data tables to compare the results with the conventional method. The conclusions are discussed in Section V.

2. The proposed method: VIS-IPT

In current section, initially, virtual signal generation is presented for voltage and current. Then, the proposed VIS-IPT is explained in detail. After that, the reference signal generation with the proposed method is given in terms of active, reactive and harmonic current components.

2.1. Virtual signal generation

Three-phase balanced signals can be written as (1). y refers to voltage (v) or current (i) components.

$$y = \begin{Bmatrix} y_A = Y_m \sin(\omega t + \phi_A) \\ y_B = Y_m \sin(\omega t + \phi_B) \\ y_C = Y_m \sin(\omega t + \phi_C) \end{Bmatrix} \tag{1}$$

where,

$$\begin{aligned} \phi_B &= \phi_A - 2\pi/3 \\ \phi_C &= \phi_A + 2\pi/3 \end{aligned} \tag{2}$$

Phase signals can be written in polar and exponential forms as follows,

$$Y_x = Y_m \angle \phi_X = Y_m e^{j\phi_x}; \quad x = A, B, C \tag{3}$$

Each phase is considered individually and rewritten as (4). $Y_{x,a}$ denotes a-component of phase x and it is the real signal.

$$Y_{x,a} = Y_m e^{j\phi_x} \tag{4}$$

In next process, symmetrical virtual signals are generated as follows. Virtual b-component can be written as (5). However, virtual b-component is delayed 120° in this form. Instead of that, virtual b-component is revised as (6). It can be seen that virtual b-component is delayed as 60° by this form [25].

$$Y_{x,b} = Y_m e^{j(\phi_x - 2\pi/3)} \tag{5}$$

The equation in (5) is written as:

$$Y_{x,b} = Y_m e^{j(\phi_x - \pi + \pi/3)} = Y_m e^{j(\phi_x + \pi/3)} e^{-j\pi} = -Y_m e^{j(\phi_x + \pi/3)} \tag{6}$$

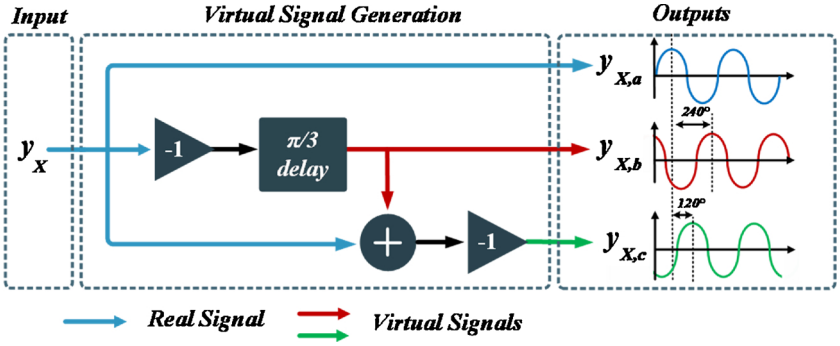

Fig. 1. Block diagram of virtual signal generation.

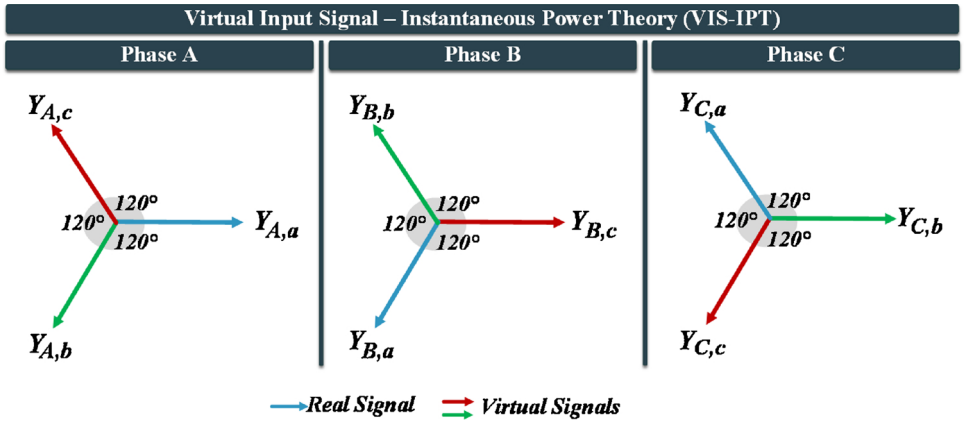

Fig. 2. Vector representation of real (blue) and virtual (green/red) signals. (For interpretation of the references to colour in this figure legend, the reader is referred to the web version of this article.)

Virtual c-component is written as (7). For symmetric electric condition, it is a common knowledge that the sum of three-phase signals is equal to zero. Since each phase is considered as an individual, the sum of real signal and its virtual symmetrical components is zero according to (8). Thus, the final equation for virtual c-component can be revised and given in (9).

The block diagram of virtual signal generation is demonstrated in Fig. 1. Besides, the vector representation of the real signals and their virtual signals are shown in Fig. 2.

$$Y_{x,c} = Y_m e^{j(\phi_x + 2\pi/3)} \tag{7}$$

$$\begin{aligned} &Y_{x,a} + Y_{x,b} + Y_{x,c} = 0 \\ &Y_{x,c} = -(Y_{x,a} + Y_{x,b}) \end{aligned} \tag{8}$$

$$Y_{x,c} = Y_m \angle(\phi_x + \pi/3) - Y_m \angle\phi_x \tag{9}$$

2.2. Virtual signal based instantaneous power

Instantaneous voltages and currents with virtual signals are written as follows. Besides, instantaneous orthogonal voltages are given as in (12).

$$v_{x,abc} = [v_{x,a} v_{x,b} v_{x,c}]^T \tag{10}$$

$$i_{x,abc} = [i_{x,a} i_{x,b} i_{x,c}]^T \tag{11}$$

$$v_{xd} = \frac{1}{\sqrt{3}} \begin{bmatrix} v_{x,bc} \\ v_{x,ca} \\ v_{x,ab} \end{bmatrix} = \frac{1}{\sqrt{3}} \begin{bmatrix} v_{x,b} - v_{x,c} \\ v_{x,c} - v_{x,a} \\ v_{x,a} - v_{x,b} \end{bmatrix} \tag{12}$$

The voltages and currents with virtual signals are transformed into $\alpha - \beta$ components by Clark–Concordia transformation. The zero component of this transformation is zero since each real signal forms a balanced condition with its virtual signals. Thus, Clark transform and inverse Clark transform matrices can be represented as,

$$T_{abc\to\alpha\beta} = \frac{2}{3} \begin{bmatrix} \cos\phi_1 & \cos\phi_2 & \cos\phi_3 \\ \sin\phi_1 & \sin\phi_2 & \sin\phi_3 \end{bmatrix} \tag{13}$$

$$T_{\alpha\beta\to abc} = \frac{2}{3} \begin{bmatrix} \cos\phi_1 & \sin\phi_1 \\ \cos\phi_2 & \sin\phi_2 \\ \cos\phi_3 & \sin\phi_3 \end{bmatrix} \tag{14}$$

where,

$$\phi_k = \frac{2\pi}{3}(k-1); \quad k = 1, 2, 3 \tag{15}$$

In this regard, the Concordia transformation of each phase is given as

$$v_{x,\alpha\beta} = T_{abc\to\alpha\beta} v_{x,abc} \tag{16}$$

$$i_{x,\alpha\beta} = T_{abc\to\alpha\beta} i_{x,abc} \tag{17}$$

In the proposed framework, instantaneous active and reactive powers of individual phase are written as (18) and (19). The zero active power is obtained as zero ($p_{x,0} = 0$) because each individual phase behaves in balanced with virtual signals.

$$p_{x,\alpha\beta} = v_{x,\alpha\beta}.\, i_{x,\alpha\beta} = [v_{x,\alpha} \quad v_{x,\beta}] \begin{bmatrix} i_{x,\alpha} \\ i_{x,\beta} \end{bmatrix} = v_{x,\alpha}.\, i_{x,\alpha} + v_{x,\beta}.\, i_{x,\beta} \tag{18}$$

$$q_{x,\alpha\beta} = v_{x,\alpha\beta} \times i_{x,\alpha\beta} = \begin{vmatrix} v_{x,\alpha} & v_{x,\beta} \\ i_{x,\alpha} & i_{x,\beta} \end{vmatrix} = v_{x,\alpha}.\, i_{x,\beta} - v_{x,\beta}.\, i_{x,\alpha} \tag{19}$$

The instantaneous active and reactive powers consist of average (dc) and oscillating (ac) parts as given below. The average parts show the powers occurring because of fundamental components. On the other hand, the oscillating parts arise from harmonic components. Oscillating parts are extracted by low pass filters.

$$p_{x,\alpha\beta} = \bar{p}_{x,\alpha\beta} + \tilde{p}_{x,\alpha\beta} \tag{20}$$

$$q_{x,\alpha\beta} = \bar{q}_{x,\alpha\beta} + \tilde{q}_{x,\alpha\beta} \tag{21}$$

The instantaneous active and reactive powers can be, as well, obtained by the following equality in *abc* frame. By this property, the instantaneous powers are calculated in *abc* frame to avoid transforming currents into $\alpha\beta$ frame.

$$p_{x,\alpha\beta} = p_{x,abc} = v_{x,abc} i_{x,abc} = v_{x,a} i_{x,a} + v_{x,b} i_{x,b} + v_{x,c} i_{x,c} \tag{22}$$

$$q_{x,\alpha\beta} = q_{x,abc} = \frac{1}{\sqrt{3}} [(v_{x,b} - v_{x,c}) i_{x,a} + (v_{x,c} - v_{x,a}) i_{x,b} + (v_{x,a} - v_{x,b}) i_{x,c}] \tag{23}$$

2.3. Compensation current generation

The current of each phase includes fundamental and non-fundamental (harmonic) components as given in following. Besides, the fundamental current comprises both active and reactive components.

$$i_x = i_{xfa} + i_{xfr} + i_{xh} \tag{24}$$

The reactive current component can be obtained in $\alpha\beta$ frame by using average reactive power as given below.

$$i_x = \begin{Bmatrix} i_{xfr,\alpha} = -\dfrac{v_{x,\beta}\bar{q}_{x,\alpha\beta}}{v^2_{x,\alpha\beta}} \\ i_{xfr,\beta} = \dfrac{v_{x,\alpha}\bar{q}_{x,\alpha\beta}}{v^2_{x,\alpha\beta}} \\ i_{xfr,0} = 0 \end{Bmatrix} \tag{25}$$

where,

$$v^2_{x,\alpha\beta} = v^2_{x,\alpha} + v^2_{x,\beta} \tag{26}$$

The harmonic current component is obtained in the same manner as follows.

$$i_{xh} = \begin{Bmatrix} i_{xh,\alpha} = \dfrac{1}{v^2_{x,\alpha\beta}}(v_{x,\alpha}\tilde{p}_{x,\alpha\beta} - v_{x,\beta}\tilde{q}_{x,\alpha\beta}) \\ i_{xh,\beta} = \dfrac{1}{v^2_{x,\alpha\beta}}(v_{x,\alpha}\tilde{q}_{x,\alpha\beta} + v_{x,\beta}\tilde{p}_{x,\alpha\beta}) \\ i_{xh,0} = 0 \end{Bmatrix} \tag{27}$$

Then, reactive current and harmonic current components are obtained in *abc* frame through inverse Clark transformation.

$$\begin{bmatrix} i_{xfr,a} \\ i_{xfr,b} \\ i_{xfr,c} \end{bmatrix} = T_{\alpha\beta\to abc}\begin{bmatrix} i_{xfr,\alpha} \\ i_{xfr,\beta} \end{bmatrix} \tag{28}$$

$$\begin{bmatrix} i_{xh,a} \\ i_{xh,b} \\ i_{xh,c} \end{bmatrix} = T_{\alpha\beta\to abc}\begin{bmatrix} i_{xh,\alpha} \\ i_{xh,\beta} \end{bmatrix} \tag{29}$$

$i_{xfr,a}$ and $i_{xh,a}$ are reactive and harmonic currents flowing on phase x. The a-component of each inverse Clark transform attributes the real component and b- and c-components are virtual signals. The virtual signals are not used in compensation. Since only the real signal will be used in compensation, it can be seen form inverse Clark transformation that the a-component is equal to α-component. Thus, Eqs. (28) and (29) can be written as (30) and (31). This means that inverse Clark transformation is not required in our framework. Moreover, β-component is not necessary to calculate the compensation signal.

$$i_{xfr,a} = i_{xfr,\alpha} \tag{30}$$

$$i_{xh,a} = i_{xh,\alpha} \tag{31}$$

The reference (compensation) signal is the summation of reactive and harmonic currents, as given in (32).

$$i_{x,com} = i_{xfr,a} + i_{xh,a} \tag{32}$$

Inserting α -components in Eqs. (25) and (27) into (32), the mathematical equation is derived as,

$$i_{x,com} = \begin{pmatrix} = \dfrac{1}{v^2_{x,\alpha\beta}}(v_{x,\alpha}\tilde{p}_{x,\alpha\beta} - v_{x,\beta}\tilde{q}_{x,\alpha\beta}) - \dfrac{1}{v^2_{x,\alpha\beta}}v_{x,\beta}\bar{q}_{x,\alpha\beta} \\ = \dfrac{1}{v^2_{x,\alpha\beta}}(v_{x,\alpha}\tilde{p}_{x,\alpha\beta} - v_{x,\beta}\tilde{q}_{x,\alpha\beta} - v_{x,\beta}\bar{q}_{x,\alpha\beta}) \\ = \dfrac{1}{v^2_{x,\alpha\beta}}(v_{x,\alpha}\tilde{p}_{x,\alpha\beta} - v_{x,\beta}q_{x,\alpha\beta}) \\ = \dfrac{1}{v^2_{x,\alpha\beta}}[v_{x,\alpha} \quad v_{x,\beta}]\begin{bmatrix} \tilde{p}_{x,\alpha\beta} \\ -q_{x,\alpha\beta} \end{bmatrix} \end{pmatrix} \tag{33}$$

3. Shunt APF with VIS-IPT control

3.1. Circuit topology

The circuit diagram of SAPF with LCL filter is demonstrated in Fig. 3. The single-phase equivalent circuit of LCL filter and its block diagram are shown in Fig. 4. v, v_i and v_{dc} are grid voltage, inverter output voltage and dc-link voltage, respectively. i_s, i_L, i_i and i_g denote source current, load current, inverter-side current and grid-side current of LCL filter, respectively. The mathematical expressions in s-domain can be written as follows.

$$\begin{Bmatrix} i_i(s) = \dfrac{1}{sL_i}(v_i(s) - v_c(s)) \\ i_g(s) = \dfrac{1}{sL_g}(v_c(s) - v(s)) \end{Bmatrix} \tag{34}$$

$$v_c(s) = \frac{1}{sC_f}(i_i(s) - i_g(s)) \tag{35}$$

The transfer function of LCL filter is obtained from these equations as (36). LCL filter has a resonance at a frequency given in (37). In order to increase the stability of the system, the resonance is damped by adding a simple resistor in series with the filter capacitor [26]. In transfer function, the equivalent series resistors (ESR) of filter inductances are ignored for mathematical analysis.

$$G(s)|_{i_g\to v_i} = \frac{1}{L_iL_gC_fs^2 + (L_i + L_g)s} \tag{36}$$

$$\omega_r = \sqrt{\frac{L_i + L_g}{L_iL_gC_f}} \tag{37}$$

3.2. System controller

The control signal of SAPF mainly includes two parts: dc-link charge and compensation of reference signals. The block diagram of the overall controller of SAPF with the proposed VIS-IPT method is illustrated in Fig. 5.

The compensation signals are obtained through the proposed VIS-IPT method. In order to acquire the signals of dc-link charge, dc voltage error signal is regulated by PI controller and then the reference dc current is transformed to abc frame from dq frame. In this study, PLL is not required in order to perform the transformation from dq to abc frame. The synchronization signal is obtained from the proposed VIS-IPT method. The transformation dq to abc frame is performed by dq to αβ matrix given in (38) and then αβ to abc matrix as given in (14).

$$T_{dq\to\alpha\beta} = \begin{bmatrix} \cos\theta_A & \sin\theta_A \\ -\sin\theta_A & \cos\theta_A \end{bmatrix} \tag{38}$$

where,

$$\theta_A = \omega t + \phi_A \tag{39}$$

In Ref. [27], the transformation functions, $cos\theta$ and $sin\theta$, are proposed to be obtained as (40) and (41) in order to avoid the grid uncertainties. These functions must change between ± 1 by synchronizing with grid frequency even under unbalanced condition. However, the functions include harmonics when unbalanced grid condition occurs.

$$\cos\theta = \frac{v_\alpha}{v_{\alpha\beta}} \tag{40}$$

$$\sin\theta = \frac{v_\beta}{v_{\alpha\beta}} \tag{41}$$

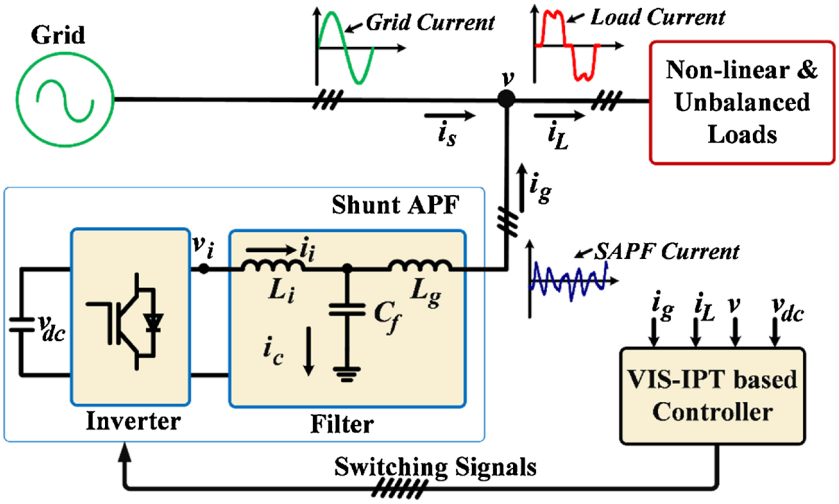

Fig. 3. Circuit diagram of SAPF with non-linear and unbalanced loads.

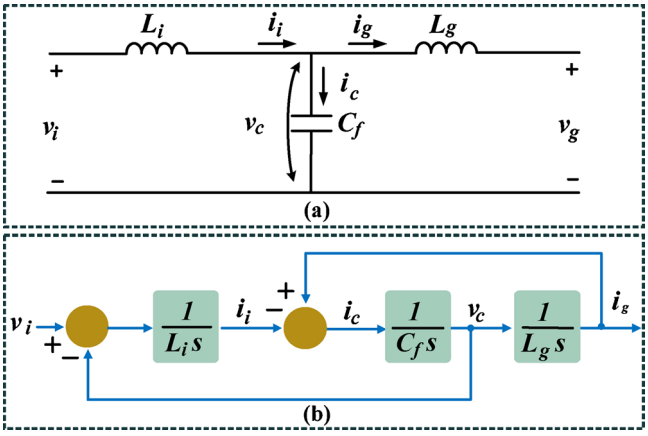

Fig. 4. Single-phase circuit and block diagram of LCL filter.

The method proposed in Ref. [27] affects the dq transformation under unbalanced state. Thus, a more accurate method is proposed in this study. The functions $cos\theta_X$ and $sin\theta_X$ in transformation (38) are obtained by the proposed VIS-IPT method as (42) and (43). Fig. 6 shows the comparison results of *cos* and *sin* functions for the methods in Ref. [27] and the proposed one under balanced and unbalanced grid conditions. It can be seen from Fig. 6 (b) that the synchronization signals are almost pure sine and cosine in the proposed method. However, the synchronization signals include a high harmonic component in the conventional method, as seen in Fig. 6 (a).

$$\cos\theta_x = \frac{v_{x,\alpha}}{v_{x,\alpha\beta}} \tag{42}$$

$$\sin\theta_x = \frac{v_{x,\beta}}{v_{x,\alpha\beta}} \tag{43}$$

The reference dc current in *abc* frame is obtained as (44) and (45). i_{dc} is obtained by controlling the dc-link voltage with PI regulator as given in (46).

$$\begin{bmatrix} i_{\alpha,dc} \\ i_{\beta,dc} \end{bmatrix} = T_{dq\to\alpha\beta} \begin{bmatrix} i_{dc} \\ 0 \end{bmatrix} \tag{44}$$

$$\begin{bmatrix} i_{A,dc} \\ i_{B,dc} \\ i_{C,dc} \end{bmatrix} = T_{\alpha\beta\to abc} \begin{bmatrix} i_{\alpha,dc} \\ i_{\beta,dc} \end{bmatrix} \tag{45}$$

$$i_{dc} = \left(k_{p,dc} + \frac{k_{i,dc}}{s}\right).(v_{ref} - v_{dc}) \tag{46}$$

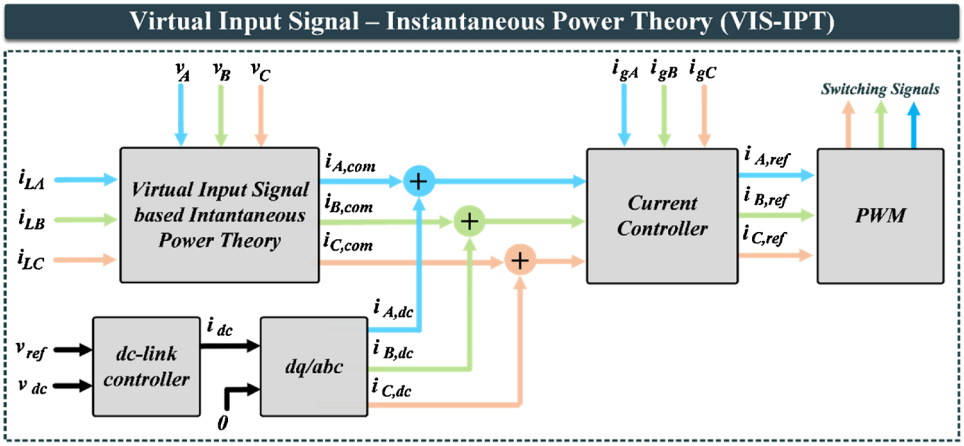

Fig. 5. Block diagram of control algorithm of SAPF with the proposed *VIS-IPT*.

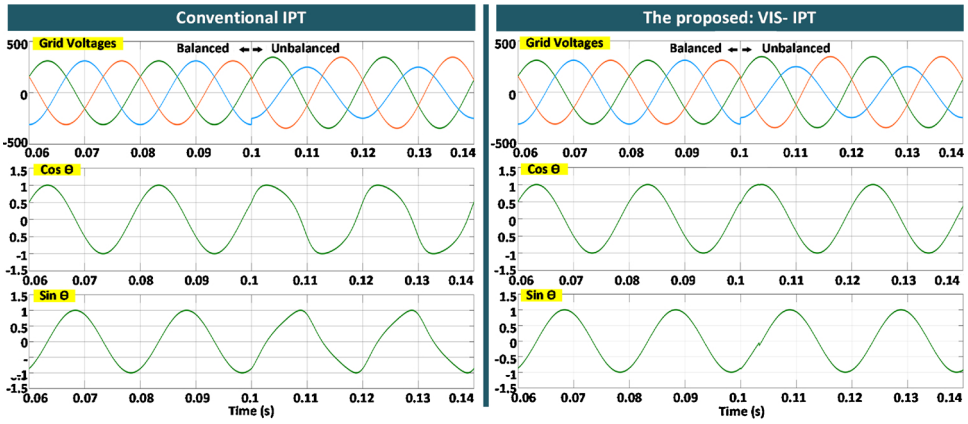

Fig. 6. Waveforms of cos and sin functions under balanced and unbalanced grid voltages with (a) Conventional method in Ref. [27] and (b) the proposed VIS-IPT method.

The reference signals of SAPF can be obtained by summing compensation reference signal and dc-link reference current as (47). In addition, this reference signal is regulated via PI controller as given in (48). The modulation signals are generated through SPWM technique.

$$\begin{bmatrix} i_{gA,ref} \\ i_{gB,ref} \\ i_{gC,ref} \end{bmatrix} = \begin{bmatrix} i_{A,com} \\ i_{B,com} \\ i_{C,com} \end{bmatrix} + \begin{bmatrix} i_{A,dc} \\ i_{B,dc} \\ i_{C,dc} \end{bmatrix} \tag{47}$$

$$i_{x,ref} = \left(k_{p,cc} + \frac{k_{i,cc}}{s}\right).(i_{gx,ref} - i_{gx}); \quad x: A, B, C \tag{48}$$

3.3. Reference generation algorithm

The proposed VIS-IPT algorithm can be summarized as follows the algorithm. Inputs: $v_{ABC} = [v_A, v_B, v_C]$, $i_{ABC} = [i_A, i_B, i_C]$ and v_{dc}.

Step 1: Generate virtual signals: $v_{X,abc} = [v_{X,a}, v_{X,b}, v_{X,c}]$ and $i_{X,abc} = [i_{X,a}, i_{X,b}, i_{X,c}]$ for $X \in \{A, B, C\}$ (This step is performed by Eqs. (6) and (9)).

Step 2: Perform Concordia transformation only for voltage signals. $v_{X,abc} \rightarrow v_{X,\alpha\beta}$ for $X \in \{A, B, C\}$.

Step 3: Calculate active and reactive powers and Extract them into oscillating and average parts. $p_{X,abc}, q_{X,abc} \rightarrow \bar{p}_{X,abc}, \tilde{p}_{X,abc}, \bar{q}_{X,abc}, \tilde{q}_{X,abc}$ (This step is performed by Eqs. (22) and (23)).

Step 4: Calculate compensating signals: $i_{X,com} = [i_{A,com}, i_{B,com}, i_{C,com}]$

Table 1
Constructed model parameters.

System	Parameter	Value
AC Grid	Grid Voltage	380 V
	Grid Frequency	50 Hz
SAPF	Rated Power	25 kVA
	Switching Frequency	20 kHz
	DC-link Voltage	650 V
LCL Filter	Inverter-side Inductance	0.5 mH
	Grid-side Inductance	0.5 mH
	Filter Capacitance	5 μF

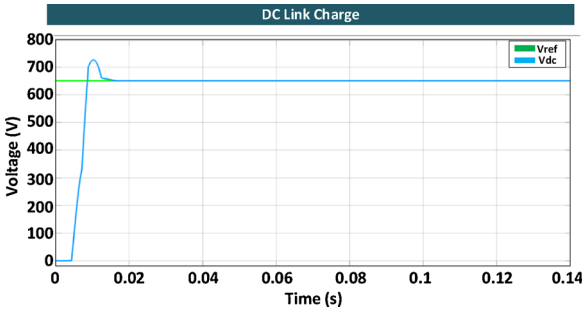

Fig. 8. Waveform of DC link charge with the proposed method.

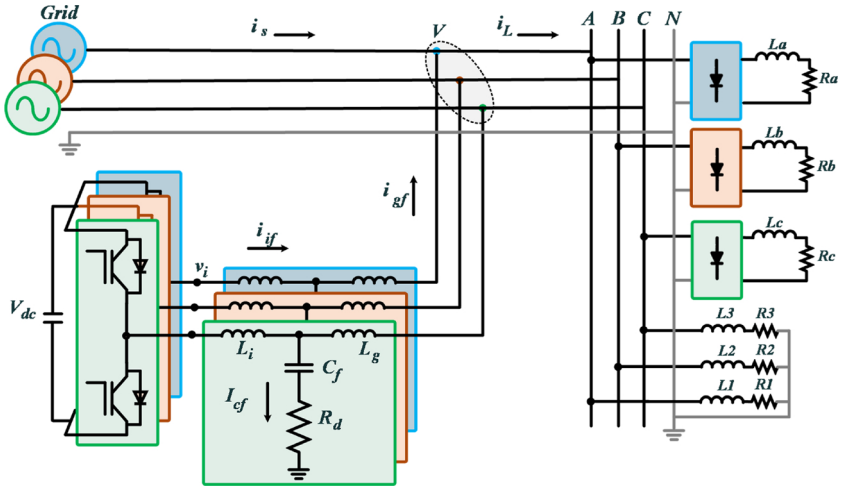

Fig. 7. Circuit diagram of tested SAPF system under unbalanced loads.

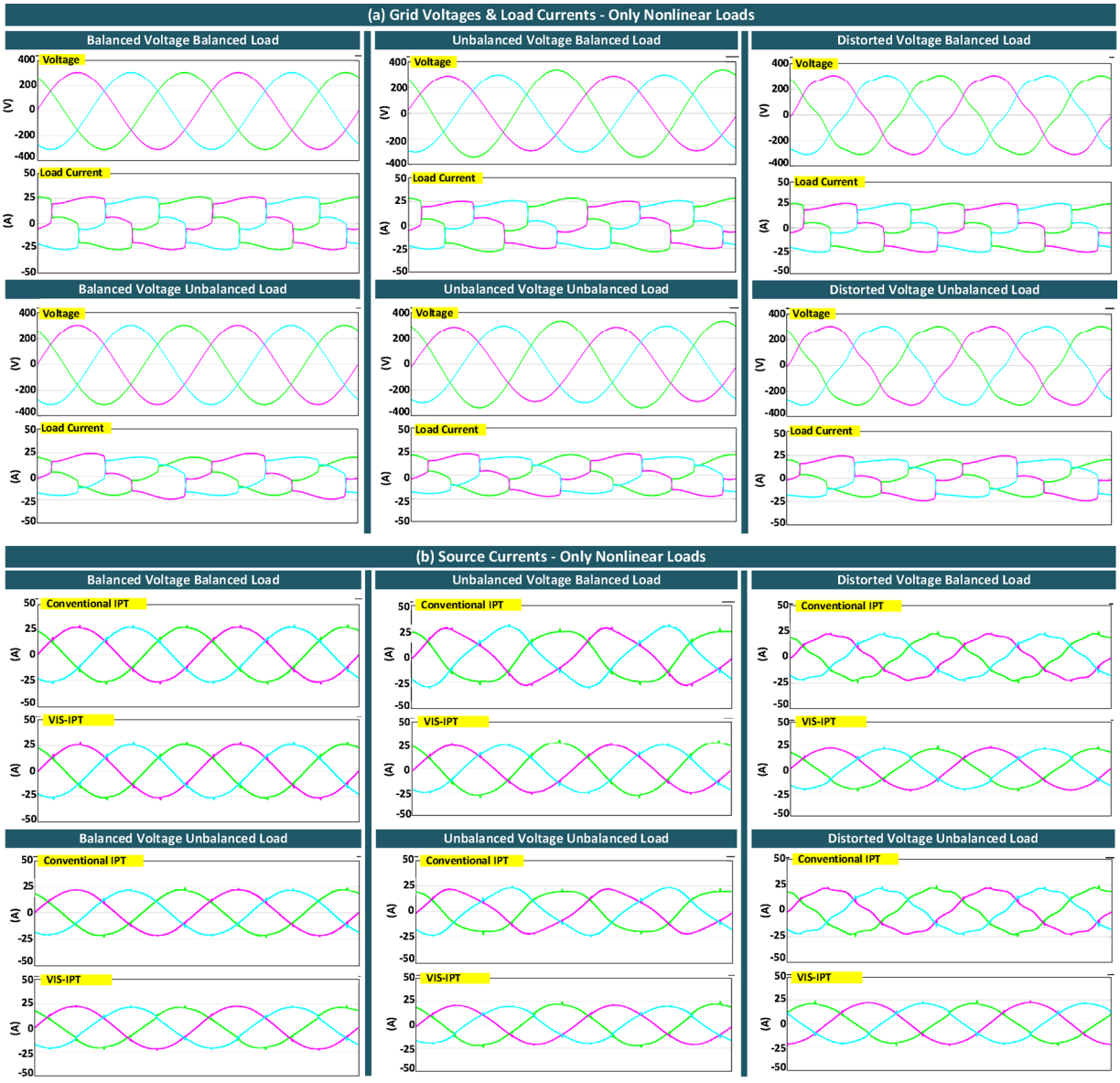

Fig. 9. Result waveforms under only nonlinear loads (a) grid voltages and load currents, and (b) source currents after the compensation with the conventional method and the proposed VIS-IPT method.

(This step is performed by Eq. (33)).

Step 5: Calculate reference dc-link charge signals: $i_{X,dc} = [i_{A,dc},\ i_{B,dc},\ i_{C,dc}]$ (This step is performed by Eqs. (44)–(46)).

Step 6: Calculate reference signals of SAPF and generate modulation reference signals: $i_{gX,ref} = [i_{gA,ref},\ i_{gB,ref},\ i_{gC,ref}]$ and $i_{X,ref} = [i_{A,ref},\ i_{B,ref},\ i_{C,ref}]$ (This step is performed by Eqs. (47) and (48)).

4. Case studies and results

In order to show the effectiveness of the proposed method, a simulation model of SAPF and unbalanced load group is constructed as demonstrated in Fig. 7. The proposed method is examined for both harmonics and reactive power compensation. Table 1 summarizes the details of the constructed model parameters.

The constructed simulation model and the proposed control algorithm are developed and investigated in Matlab/Simulink environment. In order to assess the proposed VIS-IPT method, comprehensive simulation studies are fulfilled by taking account six different cases: in case 1, balanced voltages and loads (BV-BL), in case 2, balanced voltages and unbalanced loads (BV-UL), in case 3, unbalanced voltages and balanced loads (UV-BL), in case 4, unbalanced voltages and loads (UV-UL), in case 5, distorted voltages and balanced loads (DV-BL), in case 6, distorted voltages and loads (DV-UL). In addition, all cases are examined for only harmonic current compensation and harmonic current & reactive power compensation.

To compensate harmonics and reactive components, DC link is initially charged up to the reference voltage level. The charge of DC link is performed by the proposed method as mention above. The charge of DC link is demonstrated in Fig. 8.

The waveforms of grid voltage, load current and source current after

Fig. 10. Result waveforms under nonlinear & inductive loads (a) grid voltages and load currents, and (b) source currents after the compensation with the conventional method and the proposed method.

Table 2
THD values of phases for all cases under different load types.

Load/ Case	Only nonlinear load			Nonlinear + Inductive load				Highly ınductive loads			
	Ph_A	Ph_B	Ph_C	Ph_A	Ph_B	Ph_C	PF	Ph_A	Ph_B	Ph_C	PF
BV–BL	22.81 %	22.81 %	22.81 %	13.91 %	13.91 %	13.91 %	0.79057	4.52 %	4.52 %	4.52 %	0.51068
UV–BL	21.33 %	24.66 %	25.93 %	10.62 %	12.28 %	11.81 %	0.79050	4.22 %	4.81 %	4.66 %	0.49723
BV–UL	15.84 %	22.00 %	23.94 %	6.03 %	10.92 %	11.04 %	0.78450	2.56 %	3.32 %	3.9 %	0.52455
UV–UL	15.13 %	22.38 %	23.10 %	5.78 %	10.98 %	10.39 %	0.78603	4.09 %	4.86 %	4.68 %	0.50307
DV–BL	24.88 %	24.88 %	24.88 %	12.91 %	12.91 %	12.91 %	0.77425	6.36 %	6.36 %	6.36 %	0.49837
DV–UL	18.69 %	24.32 %	26.02 %	7.58 %	12.58 %	12.40 %	0.78560	3.88 %	4.97 %	5.52 %	0.50769

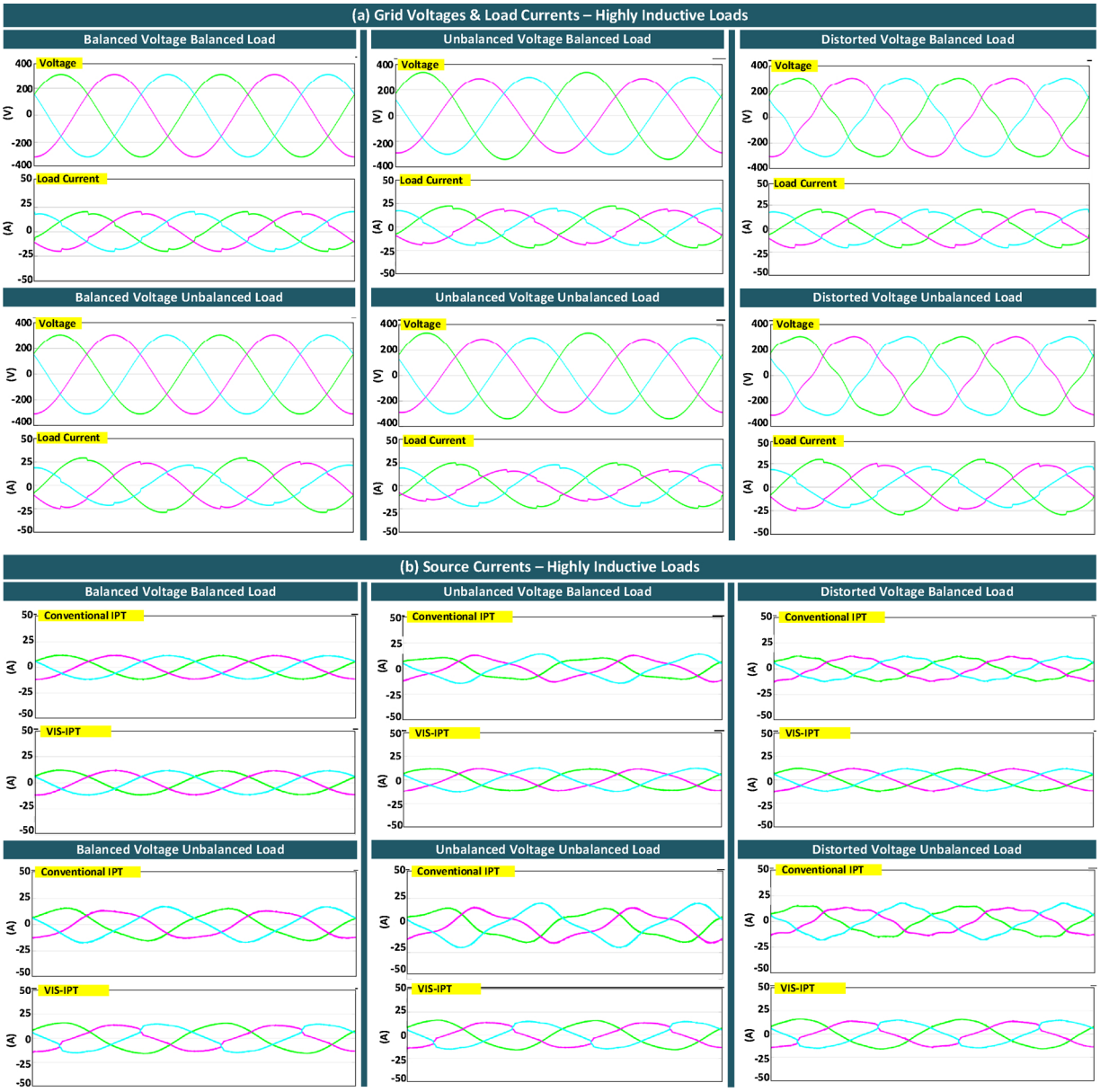

Fig. 11. Result waveforms under highly inductive loads (a) grid voltages and load currents, and (b) source currents after the compensation with the conventional method and the proposed method.

compensation are shown in Fig. 9 and Fig. 10. In addition, Table 2 demonstrates THDs of load group under different cases. The PFs of loads are also demonstrated in Table 2 for nonlinear & inductive loads. In order to constitute unbalance voltage condition, 0.1 pu negative sequence at 50° and 0.1 pu zero-sequence at 30° are included in the grid voltage. Besides, the THD of voltages is 5.6% for distorted voltage cases. The source currents after compensation with conventional (upper) and the proposed (lower) methods are illustrated under different cases by applying only nonlinear loads and nonlinear & inductive load group.

In highly inductive load groups, the proposed framework is tested and compared with conventional method. Fig. 11 shows the obtained results for highly inductive loads. The grid voltages and load currents are introduced in Fig. 11 (a) according to the different states. Fig. 11 (b) presents the source currents for conventional IPT and VIS-IPT.

The THD spectrum of case results is shown in Fig. 12. It can be seen that the proposed and conventional methods achieve sufficient compensation performance under BV-BL case. THD of source current is almost the same, for both methods under three different load types, in range of 1.9–2.2 % which satisfies limits determined in IEEE Std. 519.

In UV-BL case, THDs of source current are 10.37%, 10.96% and 9.94% for nonlinear load, 13.87%, 13.93% and 12.34% for nonlinear & inductive load and 10.59%, 7.52% and 8.45% for highly inductive loads when compensating with the conventional method. This shows that the conventional method does not satisfy the limits. In contrast, the THDs are 2.61%, 2.46% and 2.64% for nonlinear load, 4.04%, 4.07% and 4.29% for nonlinear & inductive load and 4.7%, 5.6% and 5.78% for highly inductive load with the proposed method. It is clear that the proposed method is more effective than the conventional one in this

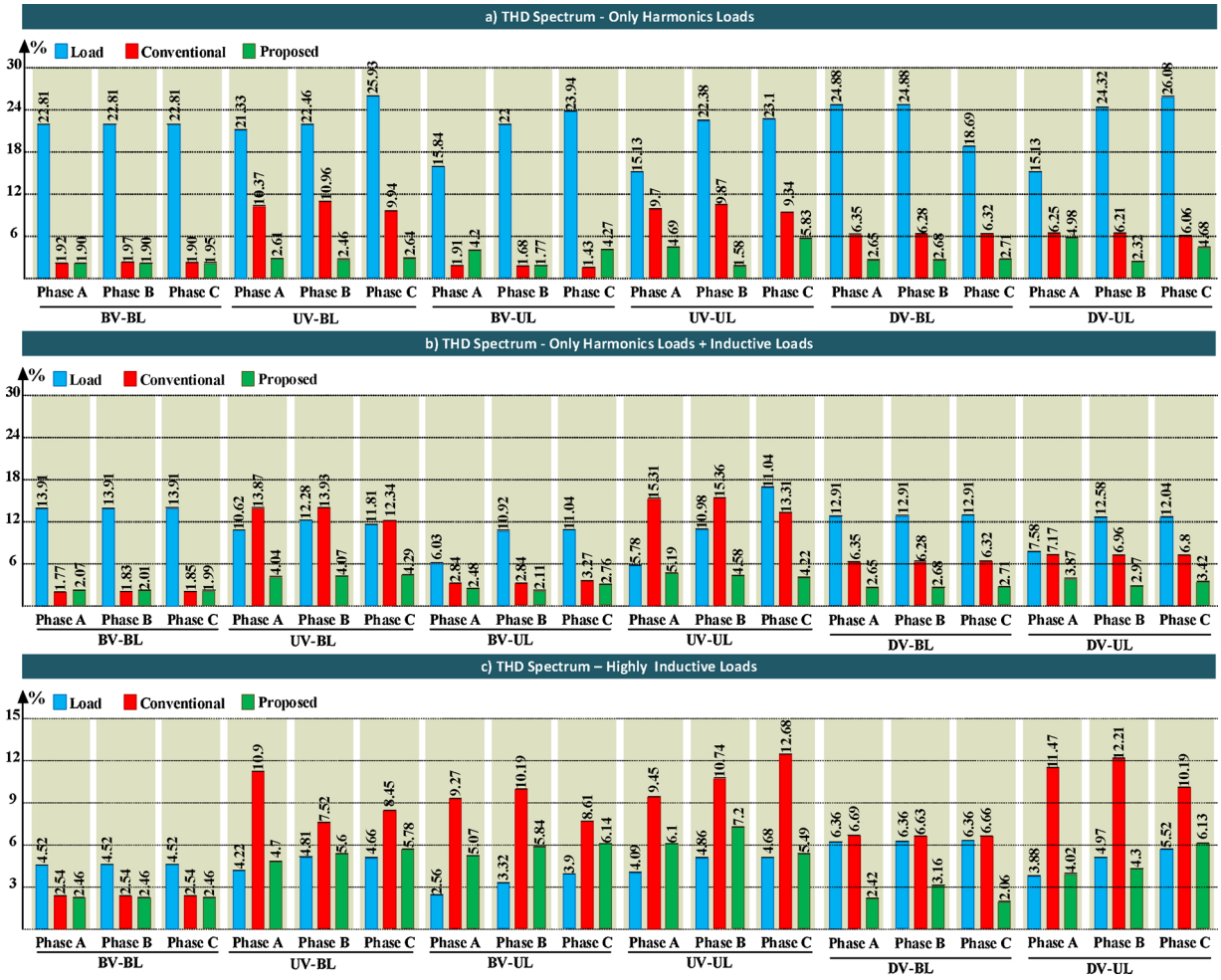

Fig. 12. THD spectrum graphics under (a) only harmonics loads, (b) nonlinear & inductive loads, and (c) highly inductive loads.

case.

In BV-UL case, THDs of source current are 1.91%, 1.68% and 1.43% for nonlinear load and 2.84%, 2.84% and 3.27% for nonlinear & inductive load and 9.27%, 10.19% and 8.61% for highly inductive loads with the conventional method. Besides, THDs are 4.2%, 1.77% and 4.27% for nonlinear load, 2.48%, 2.11% and 2.76 for nonlinear & inductive load and 5.07%, 5.84% and 6.14% for highly inductive load with the proposed method. In this case, the conventional method shows better compensation under only nonlinear load. However, the proposed method still keeps THDs of source current under the limits.

In UV-UL case, THDs of source current are 9.7%, 9.87% and 9.34% for nonlinear load, 15.31%, 15.36% and 13.31% for nonlinear & inductive load and 9.45%, 10.74% and 12.86% for highly inductive loads through the conventional method. It can be seen that THDs are increased with the conventional method under nonlinear & inductive load. The THDs are 4.69%, 1.58% and 5.83% for nonlinear load, 5.19%, 4.58% and 4.22% for nonlinear & inductive load and 6.1%, 7.2% and 5.49% for highly inductive load with the proposed method. The proposed method compensates the harmonic currents more influential than the conventional method in this situation.

In DV-BL case, THDs of source current are 6.3% for nonlinear load, 6.67% for nonlinear & inductive load and 6.66% for highly inductive loads through the conventional method, which does not satisfy the determined limits. The THDs are 2.6% for nonlinear load, 2.8% for nonlinear & inductive load and 3.16% for highly inductive loads with the proposed method. The proposed method compensates the harmonic currents more influential than the conventional method under the distorted grid voltage.

In DV-UL case, THDs of source current are 6.25%, 6.21% and 6.07% for nonlinear load, 7.17%, 6.96% and 6.8% for nonlinear & inductive load and 11.47%, 12.21% and 10.19% for highly inductive loads through the conventional method. The THDs are 5.07%, 2.32% and 4.68% for nonlinear load, 3.87%, 2.97% and 3.42% for nonlinear & inductive load and 4.02%, 4.3% and 6.13% for highly inductive load with the proposed method. The proposed method compensates the harmonic currents more effective than the conventional method under distorted voltage and unbalanced load condition.

A significant parameter for the comparison of harmonic distortion is TDD. The calculation way of TDD is given in Appendix A. TDD indicates the whole distortion index accounting for the total three-phase system. It can be seen from Fig. 13 that the proposed method demonstrates better compensation performance. The conventional method is only better in BV-UL case when only the harmonic load is active. The proposed method is more effective especially under unbalanced voltage condition.

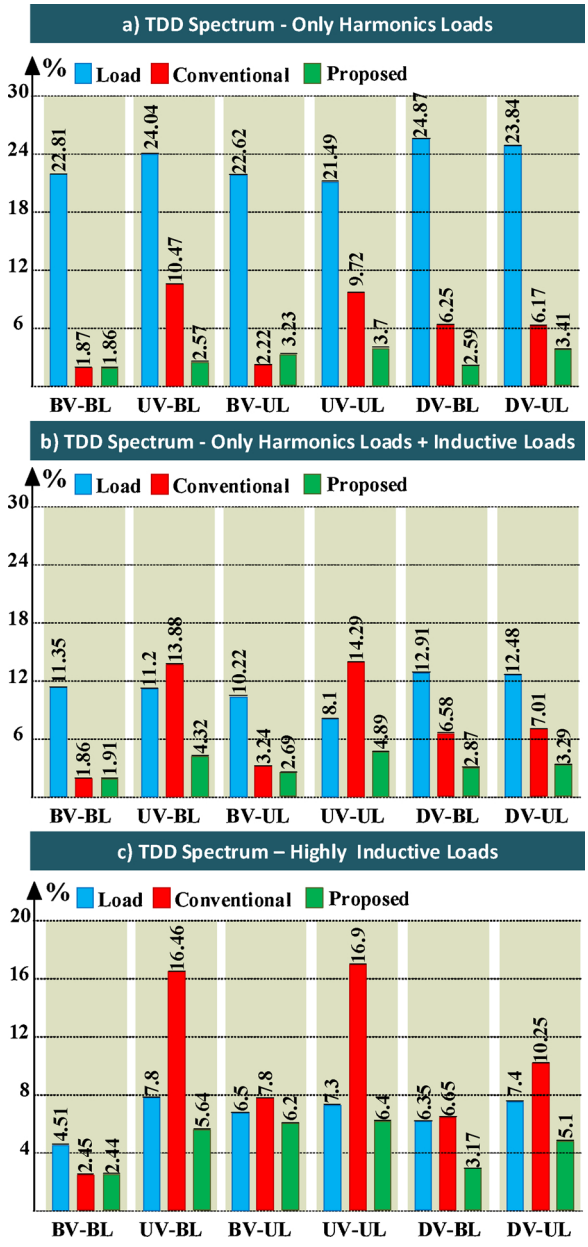

Fig. 13. TDD spectrum graphics under (a) only harmonics loads, (b) nonlinear & inductive load, and (c) highly inductive loads.

The reactive power compensation is investigated for harmonic load + inductive load. To calculate PF, effective power factor is taken into account owing to including harmonics and unbalance condition. The effective PF calculations are expressed in Appendix B. The PFs are almost 0.78 for nonlinear load & inductive and 0.5 for highly inductive loads. The PF is almost unity in both methods for all cases. However, the proposed method compensates the reactive power more effective than the conventional method, closer to unity.

5. Conclusions

In this study, a novel framework of IPT has been proposed to extract the current harmonics under balanced/unbalanced electrical conditions. In this regard, the proposed framework is based on the generation of virtual signals of current and voltage. Thus, "virtual input signal based instantaneous power theory (VIS-IPT)" terminology has been preferred in the manuscript and compared with conventional IPT scheme. In the proposed VIS-IPT method, the real and imaginary powers are calculated through the virtual signals for each phase, separately. For this, voltages/currents each phase has been considered as individually and performed in multiple frame transformation. The harmonic and reactive current components flowing on both phases are obtained for each phase, separately. Besides, the details of the proposed method have been clarified by mathematical formulations and vectorial representations.

To synchronize the SAPF to the grid, cos & sin functions used in dc-link charge have been generated by the proposed VIS-IPT method. In comparison with the conventional framework, the advantage of the proposed method is that the third harmonics have been avoided under unbalanced grid situations. Moreover, an algorithm has been introduced for reference generation via the proposed VIS-IPT method.

A variety of operational load/source case situations have been provided and examined with Simulink software to demonstrate the effectiveness of the proposed method. The proposed method has been examined with respect to THD, TDD and PF, and a comparative analysis with the traditional method has been carried out. Performance results have indicated the efficient performance for the proposed method under different load/source conditions.

Conflict of interest

None.

Acknowledgment

This study is financially supported by the Scientific Research Project Unit on Çukurova University (Project Number: FBA-2019-9760).

Appendix A

Total Demand Distortion (TDD) is calculated for three-phase system as follows.

$$TDD_{3\phi} = \frac{\sqrt{I_{THD,A}^2 I_{S,A}^2 + I_{THD,B}^2 I_{S,B}^2 + I_{THD,C}^2 I_{S,C}^2}}{I_e} \tag{49}$$

Where, THD_x given in (50) represents total harmonic distortion of current flowing on phase-X. I_e is equivalent three-phase rms current, given in (51).

$$TDD_X = \frac{\sqrt{I_{SX}^2 - I_{SXf}^2}}{I_{SX}}; \quad X = A, B, C \tag{50}$$

$$I_e = \sqrt{\frac{I_{SA}^2 + I_{SB}^2 + I_{SC}^2}{3}} \tag{51}$$

Appendix B

Effective power factor is calculated as given in (52). The active powers are calculated as (53). θ_x is phase difference between voltage and current component at phase-X. In addition, effective power is obtained as (54).

$$PF_e = \frac{P}{S_e}; \quad P = P_A + P_B + P_C \tag{52}$$

$$P_x = V_x I_x \cos\theta_x; \quad X = A, B, C \tag{53}$$

$$S_e = 3V_e I_e \tag{54}$$

Where, effective voltage and current is acquired as follows.

$$Y_e = \sqrt{\frac{Y_A^2 + Y_B^2 + Y_C^2}{3}}; \quad Y, V, I \tag{55}$$

References

[1] A. Zafari, M. Jazaeri, Conceptual design of an efficient unified shunt active power filter based on voltage and current source converters, Energy 119 (2017) 911–925.
[2] X. Liang, O. Ilochonwu, Passive harmonic filter design scheme, IEEE Ind. Appl. Mag. 17 (2011) 36–44.
[3] A. Bhattacharya, C. Chakraborty, S. Bhattacharya, Shunt compensation, IEEE Ind. Electron. Mag. 3 (2009) 38–49.
[4] I. E. Commission, IEC 61000-3-2-Electromagnetic Compatibility (EMC) - Part 3-2: Limits - Limits for Harmonic Current Emissions, ed (1998).
[5] IEEE recommended practices and requirements for harmonic control in electrical power systems, IEEE Std 519-1992, (1993), pp. 1–112.
[6] R.S. Herrera, P. Salmeron, Instantaneous reactive power theory: a comparative evaluation of different formulations, IEEE Trans. Power Deliv. 22 (January) (2007) 595–604.
[7] H. Kim, F. Blaabjerg, B. Bak-Jensen, J. Choi, Instantaneous power compensation in three-phase systems by using p–q–r theory, IEEE Trans. Power Electron. 17 (September) (2002) 701–710.
[8] C. Lascu, L. Asiminoaei, I. Boldea, F. Blaabjerg, High performance current controller for selective harmonic compensation in active power filters, IEEE Trans. Power Electron. 22 (September) (2007) 1826–1835.
[9] B. Singh, K. Al-Haddad, A. Chandra, A review of active filters for power quality improvement, IEEE Trans. Ind. Electron. 46 (October) (1999) 960–971.
[10] Y. Tang, P.C. Loh, P. Wang, F.H. Choo, F. Gao, F. Blaabjerg, Design, control, and implementation of LCL-filter-based shunt active power filters, 2011 Twenty-Sixth Annual IEEE Applied Power Electronics Conference and Exposition (APEC) (2011) 98–105.
[11] M. Mehrasa, E. Pouresmaeil, S. Zabihi, E.M.G. Rodrigues, J.P.S. Catalão, A control strategy for the stable operation of shunt active power filters in power grids, Energy 96 (2016) 325–334.
[12] R.S. Herrera, P. Salmeron, H. Kim, Instantaneous reactive power theory applied to active power filter compensation: different approaches, assessment, and experimental results, IEEE Trans. Ind. Electron. 55 (January) (2008) 184–196.
[13] W.U. Tareen, S. Mekhilef, Transformer-less 3P3W SAPF (three-phase three-wire shunt active power filter) with line-interactive UPS (uninterruptible power supply) and battery energy storage stage, Energy 109 (2016) 525–536.
[14] M. Inci, M. Buyuk, M. Tumay, FFT based reference signal generation to compensate simultaneous voltage sag/swell and voltage harmonics, 2016 IEEE 16th International Conference on Environment and Electrical Engineering (EEEIC) (2016) 1–5.
[15] A.A. Girgis, W.B. Chang, E.B. Makram, A digital recursive measurement scheme for online tracking of power-system harmonics, IEEE Trans. Power Deliv. 6 (July) (1991) 1153–1160.
[16] R.I. Diego, J. Barros, Global method for time-frequency analysis of harmonic distortion in power systems using the wavelet packet transform, Electr. Power Syst. Res. 79 (August) (2009) 1226–1239.
[17] H. Akagi, Y. Kanazawa, A. Nabae, Instantaneous reactive power compensators comprising switching devices without energy-storage components, IEEE Trans. Ind. Appl. 20 (1984) 625–630.
[18] D.A. Marshall, F.P. Venter, J.D. Vanwyk, An evaluation of the instantaneous calculation of load current components, Eur. Trans. Electrical Power Eng. 3 (January–Febuary) (1993) 53–59.
[19] N. Geddada, S.B. Karanki, M.K. Mishra, Synchronous reference frame based current controller with SPWM switching strategy for DSTATCOM applications, IEEE International Conference on Power Electronics, Drives and Energy Systems (PEDES) (2012) 1–6.
[20] M. Reyes, P. Rodriguez, S. Vazquez, A. Luna, R. Teodorescu, J.M. Carrasco, Enhanced decoupled double synchronous reference frame current controller for unbalanced grid-voltage conditions, IEEE Trans. Power Electron. 27 (September) (2012) 3934–3943.
[21] P. Verdelho, V. Soares, A unity power factor PWM voltage rectifier based on the instantaneous active and reactive current i(d)–i(q) method, Isie' 97 — Proceedings of the IEEE International Symposium on Industrial Electronics, Vols 1-3, 1997, pp. 411–416.
[22] M. Depenbrock, V. Staudt, H. Wrede, Concerning "Instantaneous power compensation in three-phase systems by using p–q–r theory", IEEE Trans. Power Electron. 19 (July) (2004) 1151–1152.
[23] A.A. Montanari, A.M. Gole, Enhanced instantaneous power theory for control of grid connected voltage sourced converters under unbalanced conditions, IEEE Trans. Power Electron. 32 (August) (2017) 6652–6660.
[24] F. Harirchi, M.G. Simoes, Enhanced instantaneous power theory decomposition for power quality smart converter applications, IEEE Trans. Power Electron. 33 (November) (2018) 9344–9359.
[25] M. Inci, K.C. Bayindir, M. Tumay, Improved Synchronous Reference Frame based controller method for multifunctional compensation, Electric Power Syst. Res. 141 (December) (2016) 500–509.
[26] M. Büyük, A. Tan, M. Tümay, K.Ç. Bayındır, Topologies, generalized designs, passive and active damping methods of switching ripple filters for voltage source inverter: a comprehensive review, Renewable Sustainable Energy Rev. 62 (2016) 46–69 9//.
[27] Y. Hoon, M.A.M. Radzi, M.K. Hassan, N.F. Mailah, Operation of three-level inverter-based shunt active power filter under nonideal grid voltage conditions with dual fundamental component extraction, IEEE Trans. Power Electron. 33 (September) (2018) 7558–7570.